Nonadiabaticity of electron-tunneling-ionization processes in elliptical strong laser fields

Jun Cai,[1,2] Yan-jun Chen,[3] Qin-zhi Xia,[2] Di-fa Ye,[2] Jie Liu,[2,4,5] and Li-bin Fu[2,4,6,*]

[1]*Jiangsu Key Laboratory of Advanced Laser Materials and Devices, School of Physics and Electronic Engineering, Jiangsu Normal University, Xuzhou 221116, China*

[2]*National Laboratory of Science and Technology on Computational Physics, Institute of Applied Physics and Computational Mathematics, Beijing 100088, China*

[3]*College of Physics and Information Technology, Shaanxi Normal University, Xi'an 710119, China*

[4]*CAPT, HEDPS, and IFSA Collaborative Innovation Center of MoE, Peking University, Beijing 100871, China*

[5]*Center for Fusion Energy Science and Technology, China Academy of Engineering Physics, Beijing 100088, China*

[6]*Graduate School, China Academy of Engineering Physics, Beijing 100193, China*

(Received 21 July 2017; published 19 September 2017)

We theoretically investigate the electron-tunneling process for a helium atom irradiated by an elliptical strong laser field. The momentum distribution for an electron ionized during the cycle when the laser intensity reaches its maximum is captured, such that we can ignore the interference between the wave packets ionized in different laser cycles and precisely determine the center of the momentum distribution. The quantum mechanical prediction of the center position is further compared to the semiclassical single-trajectory simulation as well as the experimental data. We find that the electron momentums along the minor axis of the laser polarization show good agreement with the nonadiabatic semiclassical calculation for a wide range of laser intensities, indicating the existence of a nonzero lateral momentum when the electron exits the barrier. On the other hand, the offset angles obtained by our quantum mechanical approach for different laser intensities are larger than the nonadiabatic semiclassical results, indicating the importance of the quantum effects during the electron's under-the-barrier dynamics.

DOI: 10.1103/PhysRevA.96.033413

I. INTRODUCTION

Electron ionization in an elliptically polarized strong laser field has drawn a lot of attention in recent years for its ultrashort-time measurement with attosecond resolution [1–3]. As the electron tunnels out of the barrier formed by the laser field and the Coulomb potential, it is accelerated by the laser field and then can return and recollide with the nucleus [4,5]. However, this recollision process is suppressed for the rotation of the electric vector in elliptical laser fields, especially for large ellipticity, such that the photoelectron momentum provides a direct probe of the electron-tunneling dynamics of the laser-atom interaction [6].

Electron tunneling in strong laser fields can be described as an adiabatic process, which means the neglect of the variation of the laser field when the electron moves through the barrier. It is commonly believed that the adiabatic model is valid when the Keldysh parameter [7] $\gamma = \omega\sqrt{2I_p}/E$ satisfies $\gamma \ll 1$, where ω is the laser frequency, I_p is the ionization potential, and E is the electric amplitude of the laser field. The tunneling process enters into the nonadiabatic regime when the Keldysh parameter has the intermediate value $\gamma \sim 1$ [8]. Besides the tunneling process, multiphoton absorption dominates the ionization process for weak laser intensity with $\gamma \gg 1$. For an elliptical laser field, taking into account the electric field perpendicular to the tunneling direction, Perelomov *et al.* [9] and Mur *et al.* [10] proposed a nonzero momentum perpendicular to the laser field when the electron exits the barrier. Based on this nonadiabatic assumption, it has been found both theoretically [11] and experimentally [12] that the ionization probability in a circularly polarized laser field has selectivity to the sign of the initial bound state's magnetic quantum number.

It is a hotly debated question of whether there is a positive tunneling time that the electron spends inside the binding barrier [13–18]. The experimental measurement of the tunneling delay time is realized by the attosecond angular streaking technique. The offset angle of the center of the photoelectron momentum distribution (PMD) with respect to the minor axis of the laser polarization can be obtained by both experimental measurement and semiclassical calculation such that the tunneling delay time can be extracted from the deviation of these two approaches, as the latter approach does not take into account the delay time. It has been reported that the measured tunneling delay time is of the order of tens of attoseconds, and it is compatible with the definition of Larmor time [15]. However, the experimentally measured results are based on the adiabatic laser-intensity calibration [13,14], while several studies suggested that the initial transverse momentum should not be neglected when the electron exits the barrier in an elliptical laser field [19–23].

On the other hand, conflicting results about the tunneling delay time were obtained by different theoretical approaches. Torlina *et al.* found that the deviation of the offset angles calculated by analytical R-matrix (ARM) method and numerical *ab initio* simulations is within two degrees [16], and they concluded that the tunneling process is instantaneous for the hydrogen atom. Klaiber *et al.* proposed an improved nonadiabatic model which includes a positive tunneling delay time, and the calculated offset angles coincide with experimental data [24]. In a recent paper, Ni *et al.* adopted classical calculation to back propagate the photoelectron's trajectories to a preset criterion of tunneling, and they also concluded that the tunneling delay time is close to zero [17].

The extraction of the tunneling delay time from PMD relies on the photoelectron's offset angle and the referenced semiclassical model. Previously, both in experiments [14,18]

*lbfu@iapcm.ac.cn

and in numerical calculations [20], the offset angle is obtained by a Gaussian fit of the angular momentum distribution after a radial integration of the PMD. We note that the radial integration mixes both the momentum distribution for electrons ionized during different laser cycles and the angular distribution for electrons with different energies.

In this paper, the momentum distribution for an electron ionized near the peak of the laser pulse is captured by solving the three-dimensional time-dependent Schrödinger equation (TDSE), such that the center of the PMD can be precisely determined. As the obtained momentum center represents the most probable trajectory ionized at the peak of the laser pulse, it is comparable to the semiclassical single trajectory (SCST) calculation with or without nonadiabatic assumption. Through the comparison of our quantum mechanical results and the SCST results, the nonadiabaticity of the tunneling process is validated.

II. CALCULATION METHOD

We use the generalized pseudospectral split-operator method [25] to solve the three-dimensional TDSE for a helium atom subjected in an elliptical laser field with single-active-electron approximation. The model potential of He is taken from Ref. [26]. The radial grid size is $R_{\max} = 150$ a.u., while the maximum angular momentum quantum number is up to $l_{\max} = 159$, the angular grid number is 180×360, and the time step is $\Delta t = 0.1$ a.u. In order to eliminate the reflection of the electron wave packet from the boundary and obtain the momentum space wave function, the coordinate space is split into the inner and the outer regions with the critical boundary $R_c = 50$ a.u., and the electron wave function can be written as [27,28]

$$\Psi(\boldsymbol{r},t) = \Psi^{\text{in}}(t) + \Psi^{\text{out}}(t). \tag{1}$$

The inner region wave function Ψ^{in} is propagated under the full Hamiltonian numerically, while in the outer region, the wave function is projected to momentum space for each 50 time steps:

$$C(\boldsymbol{p},t_i) = \left\langle \Psi_{\boldsymbol{p}}^{CV}(t_i) \middle| \Psi^{\text{out}}(t_i) \right\rangle. \tag{2}$$

Here, $\Psi_{\boldsymbol{p}}^{CV}(t)$ is the Coulomb-Volkov state [29–32]. Then the evolution of $C(\boldsymbol{p},t_i)$ to the end of the laser field is governed by the Volkov propagator $U_V(t_f,t_i) = \exp\{-\frac{i}{2}\int_{t_i}^{t_f}[\boldsymbol{p} + \boldsymbol{A}(t')]^2 dt'\}$ [27], such that the ionized electron wave function is obtained as

$$\Phi(\boldsymbol{p}) = \sum_i U_V(t_f,t_i) C(\boldsymbol{p},t_i). \tag{3}$$

In the SCST simulation, we use the tunnel ionization in parabolic coordinates with induced dipole and Stark shift (TIPIS) model, which takes into account Stark shift and dipole effects [3,33], to determine the initial tunneling position. In the adiabatic model, the initial momentum is set to be zero, while in the nonadiabatic model, a nonzero momentum perpendicular to the laser field is given by

$$p_{y0} = \frac{\varepsilon E}{\omega}\left[\frac{\sinh(\tau_0)}{\tau_0} - 1\right], \tag{4}$$

where $\tau_0 = -i\omega t_0$, and t_0 is the imaginary time of the electron's motion in the barrier [10,13].

The electric vector potential of the elliptical laser field used in this paper can be written as

$$\boldsymbol{A}(t) = \sqrt{\frac{I_0}{1+\epsilon^2}}\frac{f(t)}{\omega}[-\sin(\omega t)\hat{\mathbf{x}} + \epsilon\cos(\omega t)\hat{\mathbf{y}}], \tag{5}$$

where the laser frequency is $\omega = 0.062$ a.u., the laser ellipticity is $\epsilon = 0.87$, and the laser intensity I_0 ranges from 1.6×10^{14} to 6×10^{14} W/cm^2. The electric vector $\boldsymbol{E}(t)$ rotates counterclockwise and reaches its maximum when it points along the positive x axis at $t = 0$. The duration of the laser pulse is $\tau = 7$ fs, as used in the experiment [13]; the envelope of the pulse has the form $f(t) = \cos^2(\frac{\pi t}{2.74\tau})$.

III. CENTER OF PHOTOELECTRON MOMENTUM DISTRIBUTION

The electric field of the laser pulse and the photoelectron's final momentum distribution for laser intensity $I_0 = 2 \times 10^{14}$ W/cm^2 are depicted in Fig. 1. In Fig. 1(b), the plotted momentum distribution comes from an electron ionized during the whole laser pulse. The multiphoton rings, which are caused by the quantum interference between the wave packets ionized during different laser cycles, can be clearly observed. Unfortunately, the multiphoton rings mask the center position of the momentum distribution for a multicycle laser pulse in the numerical TDSE calculation.

In the single-trajectory calculation, the most probable photoelectron trajectory when the electric field reaches its maximum is taken into account. The comparable quantum mechanical calculation should refer to the momentum distribution for an electron ionized near the peak of the laser pulse. So we restrict the summation of Eq. (3) to a time window of

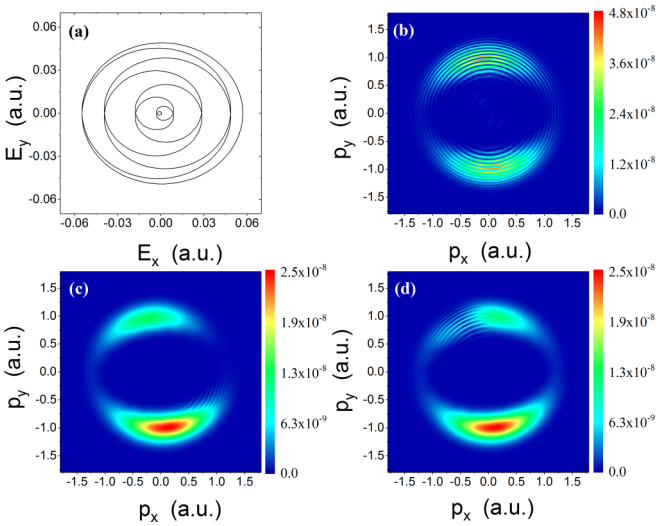

FIG. 1. (a) Illustration of the electric vector of the laser field. (b)–(d) The photoelectron momentum distribution in the $x-y$ polarization plane with $p_z = 0$. In (b), the momentum distribution refers to an electron ionized during the whole laser pulse. In (c) and (d), the momentum distributions are for the electron ionized near the laser peak, with the centers of the time window equal to $0.25T$ and $0.5T$, respectively.

one laser cycle,

$$| t_i - t_c | \leqslant 0.5T, \tag{6}$$

where t_c is the center of the time window, and $T = \frac{2\pi}{\omega}$ is the laser period. The convergence of the calculation can be verified by changing the parameter t_c, as shown in Fig. 1(c) ($t_c = 0.25T$) and Fig. 1(d) ($t_c = 0.5T$). The multiphoton rings still can be observed at different positions in these two figures; however, they do not exert influence to the momentum distribution in the lower half plane. We choose $t_c = 0.5T$ in the following calculation.

To find the momentum center in the x-y polarization plane with $p_z = 0$, a dense grid of azimuthal angle with $\Delta\theta = 0.1^\circ$ is used. The momentum when $|\Phi(\boldsymbol{p})|^2$ reaches its maximum is regarded as the center of the PMD. The photoelectron's momentum $\boldsymbol{p} = p_x\hat{\mathbf{x}} + p_y\hat{\mathbf{y}}$ and the offset angle $\theta = \arctan|\frac{p_x}{p_y}|$ can be directly obtained.

IV. NONADIABATICITY OF ELECTRON-TUNNELING PROCESS

In the attoclock experiment, the photoelectron's final momentum along the minor axis of the laser polarization p_y is used to calibrate the laser intensity with adiabatic or nonadiabatic assumptions [13]. In the theoretical study, there is no need for the laser-intensity calibration, and we can directly use p_y to validate the nonadiabaticity of the electron-tunneling process, as shown in Fig. 2(a).

In the adiabatic model, an analytic prediction of the final momentum p_y is given by

$$p_y = \frac{\varepsilon E}{\omega}, \tag{7}$$

while in the nonadiabatic model, with the existence of the initial momentum of Eq. (4), the final momentum reads as [10,13]

$$p_y = \frac{\varepsilon E}{\omega}\frac{\sinh(\tau_0)}{\tau_0}. \tag{8}$$

Taking into account the Coulomb effect after the electron exits the barrier, the SCST results of the adiabatic and nonadiabatic model are also shown in Fig. 2(a).

As can be seen in Fig. 2(a), the final momentums along the minor axis obtained by solving the TDSE (blue solid cycles) show a good agreement with the SCST results with the nonadiabatic assumption (red dashed line) for a wide range of laser intensities. We note that the discrepancy between the predictions of the adiabatic model and the nonadiabatic one is quite large (about 0.15 a.u. for the same laser intensity), while other electron-tunneling parameters, such as the tunneling delay time and the exit position, only show slight influences on the final momentum p_y. So our numerical results confirm the nonadiabaticity of the electron-tunneling process in elliptical laser fields, even for large laser intensity with Keldysh parameter $\gamma < 1$.

In Fig. 2(b), we show the offset angles obtained by the TDSE approach for different laser intensities and the comparison with the SCST results and the experimental data from Ref. [13]. Generally speaking, our TDSE results reproduce the decreasing trend of the offset angle with increasing laser

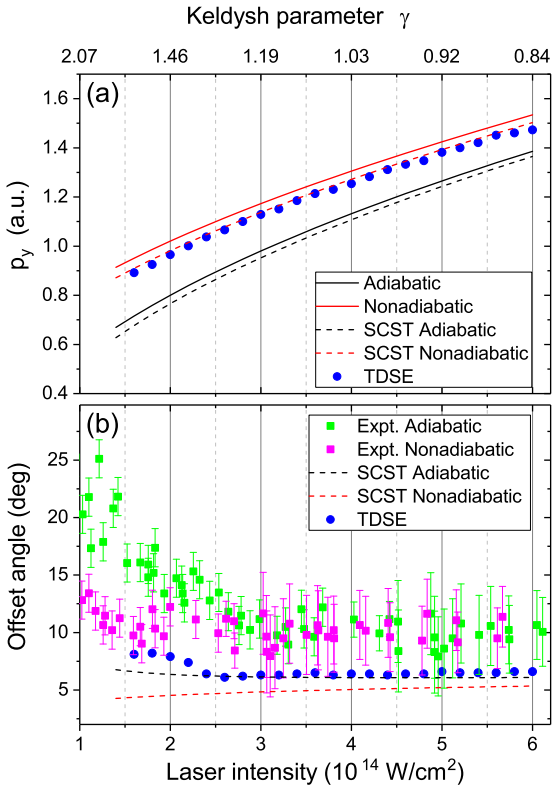

FIG. 2. (a) The final momentum along the minor axis of the laser field and (b) the offset angle. The blue cycles are the TDSE results obtained from the PMD for an electron ionized during the peak laser cycle. The black and the red solid lines are the analytical predictions of the adiabatic and the nonadiabatic models, respectively, and the dashed lines are the corresponding SCST results. In (b), the experimental results with the adiabatic (green squares) or nonadiabatic (magenta squares) laser-intensity calibration are from Ref. [13].

intensity, even though they are about 2–4 degrees smaller than the experimentally measured angles. The possible reasons for the discrepancy between our numerical results and the experimental data may be the polarization of the atom [33] and the multielectron effect [34], which are not included in our calculation. Specifically, the decreasing trend appears only for laser intensity $1.6 \times 10^{14} < I < 2.4 \times 10^{14}$ W/cm^2. It is important to point out that the experimental data with a nonadiabatic laser-intensity calibration do show a decrease in this laser-intensity range. On the other hand, the offset angles show small variations for large laser intensities both in the experimental data and in our TDSE results.

It seems that the TDSE results of the offset angle agree with the adiabatic SCST results for large laser intensities seen in Fig. 2(b). However, this agreement does not mean the validity of the adiabatic model. One reason is that the adiabatic model does not provide the correct final momentum of the photoelectron, as has been depicted in Fig. 2(a). For another reason, different from the final momentum p_y, the offset angle is quite sensitive to the electron's initial tunneling parameters. For example, the ignorance of the initial lateral momentum causes an overestimate of the the offset angle; on the opposite side, the ignorance of the tunneling delay time

leads to the underestimated results. So the agreement could be caused by the compensation of both the ignorance of the tunneling delay time and the initial lateral momentum in the adiabatic model. We suggest that the nonadiabatic model rather than the adiabatic one should be used as a reference to study the electron-tunneling process.

The offset angles predicted by the nonadiabatic SCST simulation are about 1.5° smaller than the TDSE results for large laser intensities, and this discrepancy varies up to nearly 4° for smaller laser intensity. The electron's under-the-barrier movement is fully quantum mechanical, and the quantum dynamics that are under the barrier causes the modification of the initial conditions of the classical trajectory in the continuum, including the shift of the tunnel exit coordinate [24], the tunneling delay time [18], and the longitudinal momentum [35]. The difference of the nonadiabatic SCST results and the TDSE results in Fig. 2(b) indicates the importance of the under-the-barrier quantum effects, especially in the intermediate laser-intensity region.

V. CONCLUSION

In conclusion, we studied the momentum distribution for an electron ionized near the peak of the elliptically polarized laser pulse. The calculated final momentums along the minor axis of the laser polarization show good agreement with the prediction of the SCST simulation with nonadiabatic assumption, indicating the existence of a nonzero transverse momentum when the electron tunnels through the Coulomb barrier. Our numerical results reproduce the decrease of the offset angle with increasing laser intensity; however, this decreasing trend only appears in a quite narrow laser-intensity range. The offset angles obtained by our TDSE approach are larger than the nonadiabatic semiclassical results, indicating the importance of the under-the-barrier quantum effects.

ACKNOWLEDGMENTS

We thank C. Hofmann and U. Keller for providing the experimental data. We acknowledge the kind help from X. M. Tong. This work is supported by NFRP Grant No. 2013CB834100, NNSF Grants No. 11447015, No. 11274090, No. 11404027, No. 11274051, and No. 11674034, the Research Fund of Jiangsu Normal University under Grant No. 09XLR09, and the Priority Academic Program Development (PAPD) of Jiangsu Higher Education Institutions. The calculations were performed using the resources of the High Performance Computing Center of the School of Physics and Electronic Engineering of Jiangsu Normal University.

[1] P. Eckle, M. Smolarski, P. Schlup, J. Biegert, A. Staudte, M. Schoffler, H. G. Muller, R. Dorner, and U. Keller, Nat. Phys. **4**, 565 (2008).
[2] P. Eckle, A. N. Pfeiffer, C. Cirelli, A. Staudte, R. Dörner, H. G. Muller, M. Büttiker, and U. Keller, Science **322**, 1525 (2008).
[3] A. N. Pfeiffer, C. Cirelli, M. Smolarski, D. Dimitrovski, M. Abu-samha, L. B. Madsen, and U. Keller, Nat. Phys. **8**, 76 (2012).
[4] P. B. Corkum, Phys. Rev. Lett. **71**, 1994 (1993).
[5] M. Lewenstein, P. Balcou, M. Y. Ivanov, A. L'Huillier, and P. B. Corkum, Phys. Rev. A **49**, 2117 (1994).
[6] L. Arissian, C. Smeenk, F. Turner, C. Trallero, A. V. Sokolov, D. M. Villeneuve, A. Staudte, and P. B. Corkum, Phys. Rev. Lett. **105**, 133002 (2010).
[7] L. V. Keldysh, Sov. Phys. JETP **20**, 1307 (1965).
[8] G. L. Yudin and M. Y. Ivanov, Phys. Rev. A **64**, 013409 (2001).
[9] A. M. Perelomov, V. S. Popov, and M. V. Terentev, Sov. Phys. JETP **23**, 924 (1966).
[10] V. D. Mur, S. V. Popruzhenko, and V. S. Popov, Sov. Phys. JETP **92**, 777 (2001).
[11] I. Barth and O. Smirnova, Phys. Rev. A **84**, 063415 (2011).
[12] T. Herath, L. Yan, S. K. Lee, and W. Li, Phys. Rev. Lett. **109**, 043004 (2012).
[13] R. Boge, C. Cirelli, A. S. Landsman, S. Heuser, A. Ludwig, J. Maurer, M. Weger, L. Gallmann, and U. Keller, Phys. Rev. Lett. **111**, 103003 (2013).
[14] A. S. Landsman, M. Weger, J. Maurer, R. Boge, A. Ludwig, S. Heuser, C. Cirelli, L. Gallmann, and U. Keller, Optica **1**, 343 (2014).
[15] T. Zimmermann, S. Mishra, B. R. Doran, D. F. Gordon, and A. S. Landsman, Phys. Rev. Lett. **116**, 233603 (2016).
[16] L. Torlina, F. Morales, J. Kaushal, I. Ivanov, A. Kheifets, A. Zielinski, A. Scrinzi, H. G. Muller, S. Sukiasyan, M. Ivanov, and O. Smirnova, Nat. Phys. **11**, 503 (2015).
[17] H. Ni, U. Saalmann, and J.-M. Rost, Phys. Rev. Lett. **117**, 023002 (2016).
[18] N. Camus, E. Yakaboylu, L. Fechner, M. Klaiber, M. Laux, Y. Mi, K. Z. Hatsagortsyan, T. Pfeifer, C. H. Keitel, and R. Moshammer, Phys. Rev. Lett. **119**, 023201 (2017).
[19] J.-W. Geng, L. Qin, M. Li, W.-H. Xiong, Y. Liu, Q. Gong, and L.-Y. Peng, J. Phys. B **47**, 204027 (2014).
[20] I. A. Ivanov and A. S. Kheifets, Phys. Rev. A **89**, 021402 (2014).
[21] M. Han, M. Li, M.-M. Liu, and Y. Liu, Phys. Rev. A **95**, 023406 (2017).
[22] M. H. Yuan, G. J. Zhao, and H. P. Liu, Phys. Rev. A **92**, 053405 (2015).
[23] C. L. Wang, X. Y. Lai, Z. L. Hu, Y. J. Chen, W. Quan, H. P. Kang, C. Gong, and X. J. Liu, Phys. Rev. A **90**, 013422 (2014).
[24] M. Klaiber, K. Z. Hatsagortsyan, and C. H. Keitel, Phys. Rev. Lett. **114**, 083001 (2015).
[25] X.-M. Tong and S.-I. Chu, Chem. Phys. **217**, 119 (1997).
[26] X. M. Tong and C. D. Lin, J. Phys. B **38**, 2593 (2005).
[27] X. M. Tong, K. Hino, and N. Toshima, Phys. Rev. A **74**, 031405 (2006).
[28] X.-M. Tong, J. Phys. B **50**, 144004 (2017).
[29] G. Duchateau, E. Cormier, H. Bachau, and R. Gayet, Phys. Rev. A **63**, 053411 (2001).

[30] G. Duchateau, E. Cormier, and R. Gayet, Phys. Rev. A **66**, 023412 (2002).
[31] D. G. Arbó, J. E. Miraglia, M. S. Gravielle, K. Schiessl, E. Persson, and J. Burgdörfer, Phys. Rev. A **77**, 013401 (2008).
[32] L.-Y. Peng and Q. Gong, Comput. Phys. Commum. **181**, 2098 (2010).
[33] N. I. Shvetsov-Shilovski, D. Dimitrovski, and L. B. Madsen, Phys. Rev. A **85**, 023428 (2012).
[34] A. Emmanouilidou, A. Chen, C. Hofmann, U. Keller, and A. S. Landsman, J. Phys. B **48**, 245602 (2015).
[35] J. Tian, X. Wang, and J. H. Eberly, Phys. Rev. Lett. **118**, 213201 (2017).